Structure and magnetic properties of FePt alloy cluster-assembled films

Article *in* Journal of Magnetism and Magnetic Materials · June 2004

DOI: 10.1016/j.jmmm.2003.10.028

3 authors, including:

Dong-Liang Peng
Xiamen University
178 PUBLICATIONS **2,068** CITATIONS

SEE PROFILE

T. Hihara
Nagoya Institute of Technology
201 PUBLICATIONS **1,683** CITATIONS

SEE PROFILE

Available online at www.sciencedirect.com
SCIENCE DIRECT®
Journal of Magnetism and Magnetic Materials 277 (2004) 201–208
journal of magnetism and magnetic materials
www.elsevier.com/locate/jmmm

Structure and magnetic properties of FePt alloy cluster-assembled films

D.L. Peng*, T. Hihara, K. Sumiyama

Department of Materials Science and Engineering, Nagoya Institute of Technology, Nagoya 466 8555, Japan

Received 16 September 2003; received in revised form 21 October 2003

Abstract

We studied structure and magnetic properties of Fe_xPt_{1-x} alloy clusters fabricated by a plasma-gas-condensation technique which employs two separate elemental sputtering sources and a growth chamber. Fe and Pt metal vapors generated were cooled rapidly in an Ar atmosphere, and grown into alloy clusters. Most of the as-deposited Fe_xPt_{1-x} alloy clusters are multiply twinned and have predominantly an icosahedral structure. The experimental results also show that there is a narrow distribution of the chemical composition among individual clusters but the Fe and Pt atoms are distributed homogeneously in as-deposited alloy clusters, which is discussed on the basis of a formation process of the alloy clusters in the inert gas-condensation process. The optimal magnetic hardening or the chemically ordered FCT FePt clusters can be achieved at proper annealing temperature for very short annealing time.

PACS: 61.46.+w; 75.50.Vv; 75.75.+a; 68.37.Lp; 75.30.Gw

Keywords: Fe–Pt alloy cluster; Cluster-assembled film; Plasma-gas-condensation deposition; Magnetic properties; Structure and morphology

1. Introduction

There has been a growing interest in magnetic nanoparticles in the past few years by virtue of their potential ultrahigh-density recording and medical applications [1,2]. For most applications, nanometer-sized particles or clusters serve as elemental functional units and thus their magnetic order is needed to be stable for a long time. With the decrease in the particle size, however, the magnetic anisotropy energy per particle responsible for holding the magnetic moment along certain directions becomes comparable to the thermal energy. When this happens, the thermal fluctuation induces random flipping of the magnetic moment with time, and the nanoparticles lose their stable magnetic order and become superparamagnetic. Thus, for ultrahigh-density recording, it is essential to use the media materials with high anisotropy energy. Recently, as a promising material for hard-disk drives with ultrahigh recording density, $L1_0$ structured FePt-based nonocomposite films [3–5] and chemically systhesized FePt-self-assembled nanoparticles [6–8] have attracted much attention since the equiatomic

*Corresponding author.
E-mail address: pengdl@mse.nitech.ac.jp (D.L. Peng).

0304-8853/$ - see front matter © 2003 Elsevier B.V. All rights reserved.
doi:10.1016/j.jmmm.2003.10.028

FePt alloy has extremely high magnetic anisotropy energy, K_u ($\sim 10^7$ J/m^3). However, little work has been done on Fe–Pt cluster-assembled system by the vapor-phase synthesis method [9].

In this paper, we report formation, microstructure and magnetic properties of Fe–Pt alloy clusters produced by the plasma-gas-condensation (PGC) method. The drawback of a sputter-based method employing a single alloy target is that it involves cumbersome preparation of alloy materials, which are often difficult to process mechanically. We thus employed a two-target sputtering system in order to generate and control independently the amounts of Fe and Pt metallic vapors. Our results show that it is indeed possible to fabricate alloy clusters for a relatively wide composition range. For as-deposited samples, size-monodispersed Fe–Pt alloy clusters with a disordered FCC structure were observed although formation of posited alloy clusters with the ordered structure ($L1_0$) is highly desired from an application point of view. It was found that the high-anisotropy $L1_0$ FePt phase was obtained by annealing at 600°C for 10 min.

2. Experimental

Since metal vapors are produced by sputtering of a target material, a wide variety of elements can serve as source materials [10]. We prepared the samples by using the PGC-type cluster beam deposition apparatus [11], which is based on plasma-glow-discharge vaporization (sputtering) and inert gas-condensation techniques. The apparatus is composed of three main parts: sputtering, cluster growth, and deposition chambers. We used a magnetron sputtering system with Fe and Pt targets of 80 mm diameter, controlled independently for the generation of metal vapors. The two targets were placed face to face, separated by 100 mm distance. The input power of each target was controlled in the range 50–150 W. A large amount of Ar gas of 300–400 standard cubic centimeters per minute (sccm) was introduced continuously into the sputtering chamber, making the pressure inside the chamber approximately 1.5–1.7 Torr. The vaporized Fe and Pt atoms in the sputtering chamber are decelerated by collisions with Ar gas and swept into the cluster growth room, which is cooled by liquid nitrogen. The clusters formed in this room are ejected from a small nozzle by differential pumping and a part of the cluster beam is intercepted by a skimmer, and then deposited onto a sample holder in the deposition chamber (10^{-5}–10^{-4} Torr). The effective film thickness of the deposited clusters, t_e, was estimated using a quartz crystal thickness monitor, which measures the weight of the deposited clusters and adopts the density of the bulk Fe–Pt alloy. For the present PGC-type cluster beam deposition method, roughly speaking, the actual thickness of deposited clusters, t_a, estimated from cross-sectional scanning electron microscope (SEM) image is about $t_a = 4 \times t_e$ because of a random stacking of the clusters and a porous structure of cluster-assembled films. Heat treatment of as-deposited samples was carried out in a gas pressure of about 2×10^{-6} Torr and with a heating rate of 30°C/min.

We used three kinds of substrates for the Fe–Pt cluster deposition: carbon-coated colodion films supported by Cu microgrids for transmission electron microscope (TEM) observation, silicon wafers for SEM observation, and quartz plates for magnetic measurements. We used a Hitachi HF-2000 FE-TEM operating at 200 kV for structural characterization and a Hitachi S-4700 FE-SEM operating at 15 kV. The FE-TEM was equipped with energy-dispersive X-ray (EDX) spectroscopy, which was used for compositional analyses. Magnetic measurement was performed using a superconducting quantum interference device magnetometer between 5 and 300 K in magnetic fields up to 50 kOe.

3. Results

3.1. Formation and microstructure of Fe_xPt_{1-x} alloy clusters

Fig. 1 shows bright field TEM images of the clusters with effective thickness $t_e = 1.5$–2.5 nm prepared at (a) the Ar gas flow rate: $R_{Ar} = 300$ sccm, the electric power of Pt: $P_{Pt} = 100$ W,

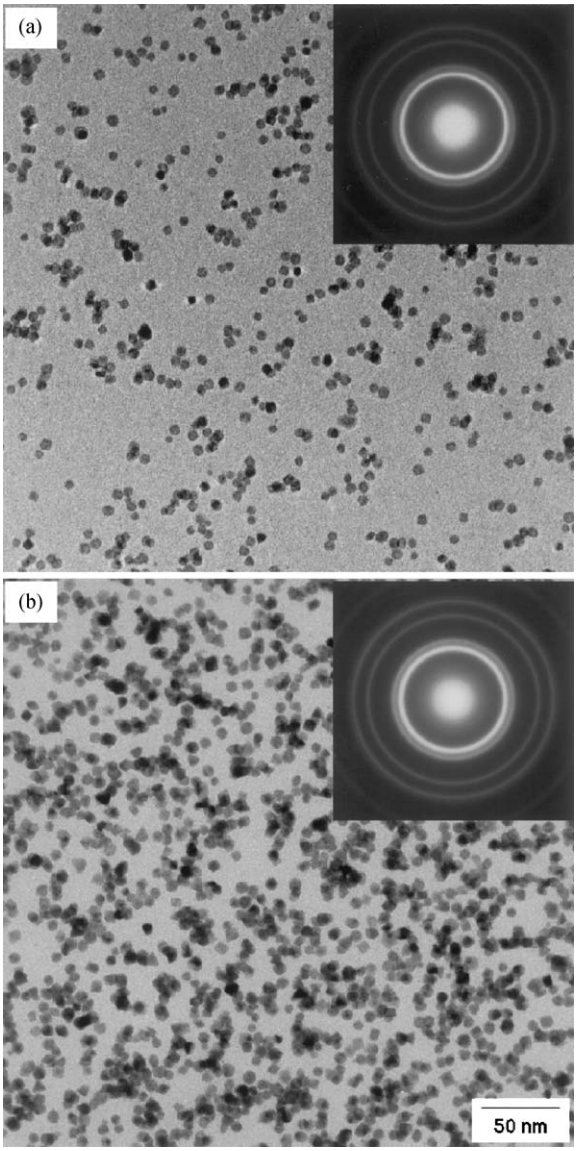

Fig. 1. Bright-field TEM images and ED patterns (insets) of as-deposited (a) $Fe_{51}Pt_{49}$ and (b) $Fe_{49}Pt_{51}$ alloy clusters with the mean cluster size $d \approx 7$ and 9 nm, corresponding to Ar gas flow rate: $R_{Ar} = 300$ and 400 sccm, respectively.

and the electric power of Fe: $P_{Fe} = 50$ W, and (b) $R_{Ar} = 400$ sccm, $P_{Pt} = 150$ W, and $P_{Fe} = 105$ W, corresponding to Fe content of $x = 51$ and 49 at%, respectively. Most of the clusters are sphere-like in shape. Using an image-analysis software (Image-Pro PLUS: Media Cybernetics), we estimated the size distributions of clusters not touching and overlapping each other in the digitized images recorded by a slow scan CCD camera in the object area of 350×350 nm^2. The estimated mean cluster diameters are $d \approx 7$ and 9 nm with a standard deviation less than 12% of d for two samples, respectively. The electron diffraction (ED) patterns (insets) observed for cluster assemblies with $t_e \approx 30$ nm can be ascribed to a high-temperature disordered FCC Fe–Pt alloy phase. This result suggests that the nonequilibrium nature of Fe–Pt alloy cluster formation in the vapor phase is the same with the observed results for the Fe–Pt alloy films [4,12,13] or nanoparticles [6–8] obtained by other methods.

Fig. 2(a) shows the average composition (C_{Fe}) of the cluster aggregates determined by EDX analysis, where the electron beam was spread with a diameter of more than 500 nm. It is seen that the composition of clusters can be easily controlled by changing the relative electric power of the two targets and R_{Ar}. As expected, the Fe content of clusters increases as P_{Fe} increases. It was also found that the average composition of the cluster aggregates changes nonlinearly with the applied power and it becomes unchanged when P_{Fe} is lower than 90 W for $R_{Ar} = 400$ sccm.

The compositions of individual clusters with $d \approx 9$ nm were also analyzed for the cluster assembly with average composition was 53 at% Fe. We randomly selected 36 different clusters and took the EDX spectra by nanoelectron beams. The estimated compositions are shown as a histogram in Fig. 2(b). The chemical compositions of these clusters exhibit a narrow peak at ~ 53 at% Fe, which is consistent with the average composition (namely EDX spectrum taken with the spread beam).

We further carried out high-resolution TEM (HRTEM) observation on as-deposited alloy clusters. These results indicated that the majority of the alloy clusters are icosahedral and/or a multiply twinned (MT) structures, which is similar to the results obtained by Stappert et al. [9] in the gas-phase sintered FePt nanoparticles. Figs. 3(a)–(d) show typical HRTEM images of the $Fe_{53}Pt_{47}$ clusters. Their diffractograms obtained from Fourier transformation of the original images are shown in Figs. 3(a′)–(d′). Clearly, the cluster of

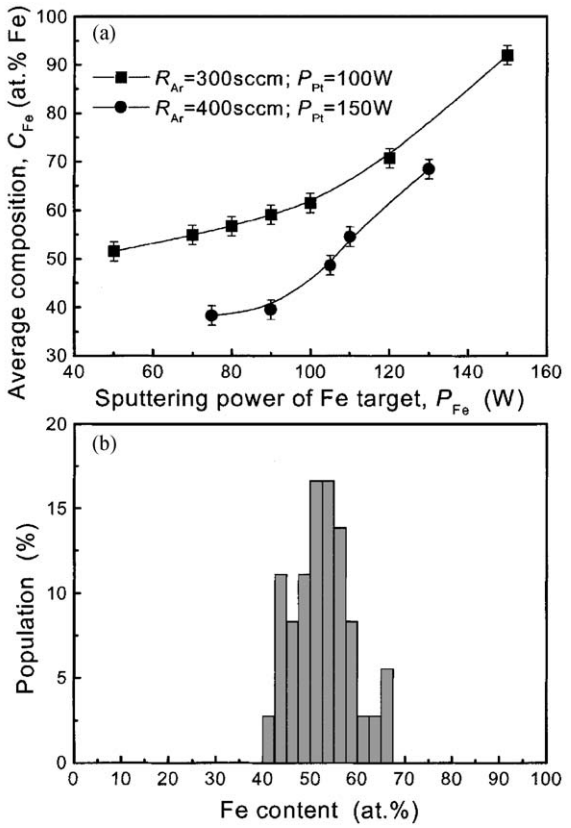

Fig. 2. (a) Average composition (C_{Fe}) of Fe–Pt cluster aggregates as a function of sputtering power of Fe target (P_{Fe}), with fixed powers of Pt target: $P_{Pt} = 100$ W for $R_{Ar} = 300$ sccm, and $P_{Pt} = 150$ W for $R_{Ar} = 400$ sccm. (b) A chemical composition histogram evaluated from the nanobeam EDX spectra of 36 individual Fe–Pt clusters. The analyzed cluster aggregate has an average composition of 53 at% Fe from EDX spectrum taken with the spread beam.

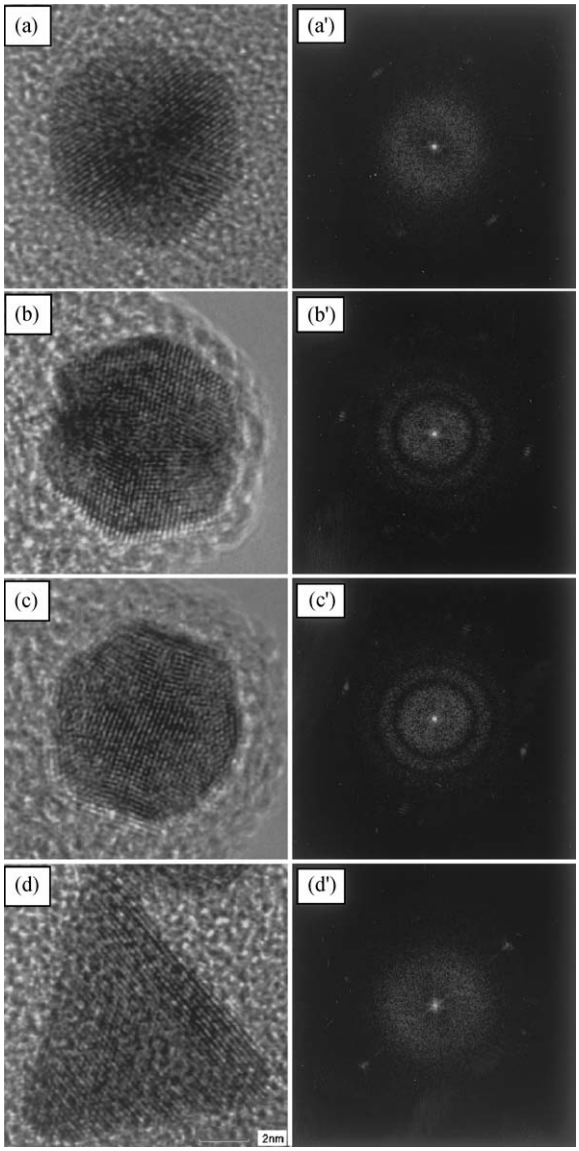

Fig. 3. HRTEM images (a–d) of as-deposited $Fe_{53}Pt_{47}$ alloy clusters and diffractograms of the images (a′–d′) as obtained from Fourier transformation of the left original images.

Fig. 3a shows a 3-fold morphological symmetry while the clusters of Figs. 3(b) and (c) have 2-fold symmetry structures. The observed icosahedral structures are similar to the images obtained by a computer simulation for icosahedral clusters [14]. Additionally, as shown in Fig. 3(d), we also observed minor clusters with a tetrahedron shape in the obtained alloy clusters. These results indicate that the as-deposited FePt alloy clusters have the same structure characteristics with the single element FCC-metallic clusters which often show the mixture of MT structures as icosahedral and decahedral in the nm sizes [15]. These MT structures do not obey the crystallographic translation symmetry rule and are completely different from those of their bulk structures. In general, the minimum energy shape for a given volume is determined by the Wulff construction which gives the equilibrium shape of a free-floating small particle, and is mathematically equivalent to stating that the normal distance from a common

center to any given surface facet is proportional to the surface free energy of the facet. Therefore, these MT structures are generally metastable and the most stable form can be obtained by annealing the clusters at a high temperature.

3.2. Morphology and phase transformation of FePt alloy cluster-assembled films

In Section 3.1, we have described the formation of Fe_xPt_{1-x} alloy clusters and the microstructure of individual alloy clusters. Here, we display the morphology and high-temperature phase transformation of the alloy cluster-assembled films, namely heavily stacked alloy cluster assemblies. Fig. 4 shows bright field TEM images ((a) as-deposited; (b) post-annealed) and corresponding ED patterns (a′ and b′) of $Fe_{49}Pt_{51}$ alloy cluster-assembled film with a thickness of $t_e = 30$ nm. After annealing the sample at 600°C for 60 min, the ED patterns (Figs. 4(a′) and (b′)) verify that the structure of the FePt cluster-assembled films has transformed from FCC γ-FePt to FCT $L1_0$-FePt. Comparing TEM images of the as-deposited and post-annealed films, it can be seen that the cluster size is slightly increased. This is attributed to cluster–cluster coalescence during high-temperature annealing.

Fig. 5 shows SEM images of the $Fe_{49}Pt_{51}$ alloy cluster-assembled film with an initial cluster size of $d \approx 9$ and a thickness of $t_e = 50$ nm: (a) as-deposited; (b) post-annealed (600°C for

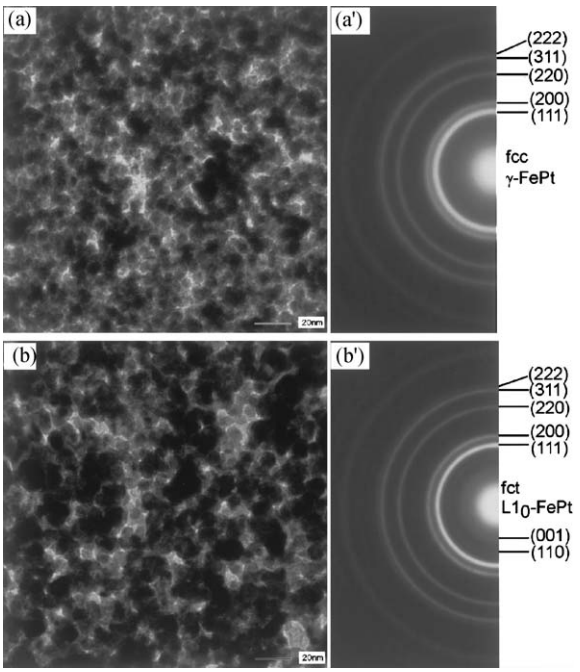

Fig. 4. TEM images and ED patterns of the $Fe_{49}Pt_{51}$ alloy cluster-assembled film ((a) and (a′): as-deposited; (b) and (b′) post-annealed at 600°C for 60 min). The film thickness is $t_e = 30$ nm.

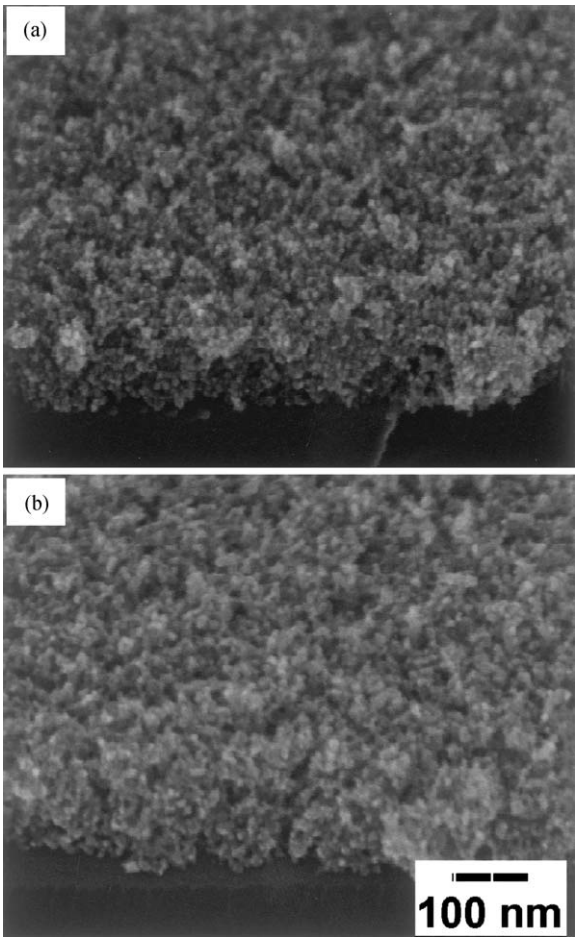

Fig. 5. SEM images of the $Fe_{49}Pt_{51}$ alloy cluster-assembled films: (a) as-deposited and (b) post-annealed at 600°C for 60 min. They were taken along a direction which has an angle of 45° with the film surface or cross-section. The film thickness is $t_e = 50$ nm.

60 min). In order to observe simultaneously the information of surface and the cross-section of the films, the SEM images were taken along a direction whose tilted angle is 45° from the film surface or the cross-section. For both as-deposited and post-annealed films, we observe a random stacking of the alloy clusters and a porous structure.

3.3. Magnetic properties

Fig. 6 shows $M-H$ loops of the as-deposited $Fe_{51}Pt_{49}$ and $Fe_{49}Pt_{51}$ cluster-assembled films with an effective thickness of $t_e \approx 50$ nm, and the mean cluster sizes of (a) $d = 7$ and (b) $d = 9$ nm, respectively. The insets of Fig. 6 show the zero-field-cooled (ZFC) and field-cooled (FC) magnetization as a function of temperature from 300 to 5 K. $Fe_{51}Pt_{49}$ film (Fig. 6(a)) is superparamagnetic at room temperature: the blocking temperature is about $T_B = 160$ K. For $Fe_{49}Pt_{51}$ film (Fig. 6(b)), the ZFC thermomagnetic curve reveals a high blocking temperature ($T_B = 270$ K) but the room-temperature magnetization curve shows a small coercivity value ($H_c \approx 25$ Oe). Such a room-temperature superparamagnetism and small coercivity value also indicate that the as-deposited FePt alloy clusters are not chemically ordered FCT structures.

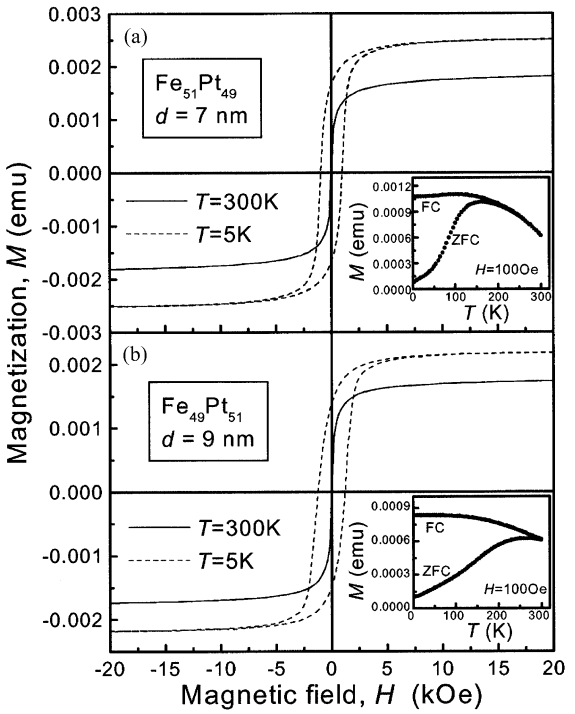

Fig. 6. Hysteresis loops of as-deposited (a) $Fe_{51}Pt_{49}$ and (b) $Fe_{49}Pt_{51}$ cluster-assembled films with an effective thickness of $t_e \approx 50$ nm and mean cluster sizes of $d = 7$ and 9 nm, respectively. The insets show the low-field thermomagnetic curves measured with increasing temperature after ZFC and FC the samples from 300 to 5 K.

In order to get an $L1_0$ ordered phase from the disordered films, we carried out heat treatment for the as-deposited cluster-assembled films. Fig. 7 shows $M-H$ loops of $Fe_{49}Pt_{51}$ alloy cluster-assembled films with an effective thickness of $t_e \approx 50$ nm and an original mean cluster size of $d = 9$ nm which were annealed for 60 min at 500, 600, 700, and 800°C. When annealing temperature (T_{an}) is lower than 500°C, H_c did not exhibit remarkable change ($H_c < 200$ Oe). When T_{an} becomes higher than 500°C, H_c increases rapidly as T_{an} increases from 500 to 700°C, and a maximum value of $H_c \sim 14$ kOe appears at 700°C. However, H_c decreases when T_{an} higher than 800°C. A similar result was observed in Fe–Pt nanoparticle assemblies by chemical synthesis and attributed to

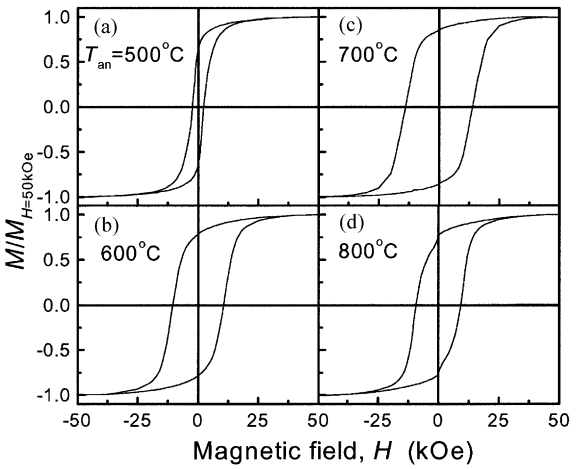

Fig. 7. Hysteresis loops of post-annealed $Fe_{49}Pt_{51}$ alloy cluster-assembled films with an effective thickness of $t_e \approx 50$ nm and an original mean cluster size of $d = 9$ nm. The as-deposited samples were annealed for 60 min at (a) $T_{an} = 500$°C, (b) 600°C, (c) 700°C, and (d) 800°C, respectively.

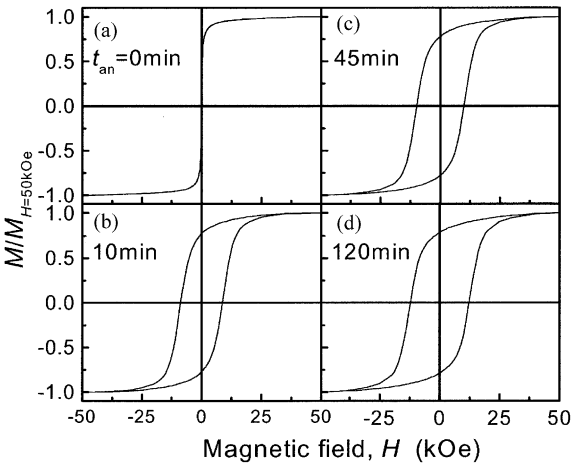

Fig. 8. Annealing time (t_{an}) dependence of hysteresis loops for an $Fe_{49}Pt_{51}$ alloy cluster-assembled film with an effective thickness of $t_e \approx 50$ nm and an original mean cluster size of $d = 9$ nm. Annealing temperature is fixed at $T_{an} = 600°C$.

excessive interparticle exchange coupling due to particle–particle coalescence at higher temperatures [8].

Fig. 8 shows M–H loops of an $Fe_{49}Pt_{51}$ alloy cluster-assembled film with an effective thickness of $t_e \approx 80$ nm and an original mean cluster size of $d = 9$ nm which was annealed at 600°C for 0, 10, 45, and 120 min, respectively. As compared with very small H_c value of the as-deposited film (Fig. 8(a)), H_c abruptly reaches about 9 kOe after annealing for only 10 min (Fig. 8(b)). After first annealing for 10 min, H_c increases gradually as t_{an} increases (Figs. 8(c) and (d)). H_c value reaches 12.2 kOe after 120 min annealing.

4. Discussion

We have demonstrated that alloy clusters can be formed using the gas-condensation technique, and that the use of two separate sputtering targets (Fe and Pt) as sources of metal vapors is effective to control the alloy cluster composition. However, it is noted that the alloy clusters obtained have a slight distribution of the chemical composition among individual clusters (Fig. 2(a)). Here, we simply discuss the formation process of the alloy clusters. In the inert gas-condensation process, vaporized metal atoms from the targets rapidly lose their kinetic energy by collisions with the inert gas atoms. The first cluster growth stage is embryo formation by thermodynamical fluctuation through three-body collisions of metal and inert gas atoms and adhesion of metal atoms [16]. These embryos are so small that they easily evaporate instead of growing to larger clusters. Only when they become larger than the critical size, the cluster growth is promoted as predicted in the classical nucleation and growth theory [17,18]: such a cluster grows step by step with absorption of atoms arriving at the surface and by cluster–cluster collisions or coagulation.

The cluster formation process in the PGC method is also basically similar to that in a colloidal particle formation process. In the latter, the following two conditions must satisfy to obtain size-monodisperse particles [19]: (1) distinct separation between nucleation and growth periods, (2) inhibition of coagulation of growing particles. In the present study, the size-monodispersed FePt alloy clusters have been obtained (Fig. 1). Therefore, the cluster growth of the alloy clusters can be considered to result mainly from formation process by absorption of atoms arriving at the surface of growing clusters other than by cluster–cluster collisions. In fact, the HRTEM observation showed that individual as-deposited alloy clusters on the TEM microgrid are homogeneous although most of them have an MT structure. Moreover, the ED patterns of the as-deposited alloy cluster assemblies (Fig. 1) showed a single disordered FCC Fe–Pt alloy phase. These results clearly suggest that the Fe and Pt atoms are homogeneously distributed in the alloy clusters. Therefore, the transformation from a disordered FCC to an ordered FCT phase occurred in a very short time (<10 min), leading to a large H_c.

We further analyzed the magnetic anisotropy for the as-deposited alloy cluster-assembled films. As shown in the insets of Fig. 6, both samples have blocking temperatures ($T_B = 160$ and 270 K) lower than room temperature. The relationship between the uniaxial anisotropy K_u and the cluster volume V is given by

$$K_u = 25 k_B T_B / V. \quad (1)$$

Here, k_B is the Boltzmann constant. Using Eq. (1), the value of K_u is estimated to be 3.1×10^5 and 2.4×10^5 J/m^3 for the samples with $d = 7$ and 9 nm, respectively. These values are very small compared to the anisotropy constant of the $L1_0$ ordered FePt phase ($K_u = 6.6$–10×10^6 J/m^3). It is seen that the value of K_u decreases as the alloy cluster diameter is increased. Moreover, these values are larger by an order of magnitude than the bulk Fe ($K_1 \approx 5 \times 10^4$ J/m^3), similar to pure Fe cluster-assembled films [20]. In the case of the Fe cluster-assembled films, such an enhancement of the effective anisotropy is ascribed to the large surface anisotropy effects of the clusters and the low cluster-packing fraction of the cluster assemblies.

5. Conclusion

The formation, structural and magnetic properties of Fe_xPt_{1-x} alloy clusters have been investigated. Nearly size-monodispersed disordered Fe–Pt alloy clusters in the composition range of 39–70 at% Fe were produced using a PGC technique. The composition and size of the alloy clusters was controlled by adjusting the relative electric power of the two targets and the Ar gas flow rate. The majority of the alloy clusters are of predominantly icosahedral and/or MT structures. The experimental results also show that the Fe and Pt atoms are distributed homogeneously in the as-deposited alloy clusters which have a narrow distribution in the chemical composition. The optimal magnetic hardening or the chemically ordered FCT FePt clusters can be achieved at proper annealing temperature and short annealing time. For $Fe_{49}Pt_{51}$ cluster-assembled films, high coercivity (8.8 kOe) was obtained by annealing at 600°C within 10 min due to improvement of the chemical ordering, although as-deposited cluster-assembled films have lower blocking temperatures than room temperature. However, such a heat treatment process also leads to loss of size-monodispersiveness of the alloy clusters due to cluster–cluster coalescence. Therefore, solving this problem is a challenge for our further studies.

Acknowledgements

We appreciate Mr. H. Kurebayashi for his help with the sample preparation. This work has been supported by Grant-in-aid for Intellectual Cluster Project supported by the Ministry of Education, Science, Culture and Sports, Japan, Aichi Prefecture and Aichi Science and Technology Foundation. One of the authors (D.L. Peng) appreciates the financial support from Japan Society for the Promotion of Science (JSPS).

References

[1] A.S. Edelstein, R.C. Cammarata (Ed.), Nanomaterials: Synthesis, Properties and Applications, Institute of Physics, Bristol, 1996.
[2] J.I. Martín, J. Nogués, K. Liu, J.L. Vicent, I.K. Schuller, J. Magn. Magn. Mater. 256 (2003) 449.
[3] J.P. Liu, C.P. Luo, Y. Liu, D.J. Sellmyer, Appl. Phys. Lett. 72 (1998) 483.
[4] C.P. Luo, S.H. Liou, L. Gao, Y. Liu, D.J. Sellmyer, Appl. Phys. Lett. 77 (2000) 2225.
[5] H. Zeng, M.L. Yan, N. Powers, D.J. Sellmyer, Appl. Phys. Lett. 80 (2002) 2350.
[6] S. Sun, C.B. Murray, D. Weller, L. Folks, A. Moser, Science 287 (2000) 1989.
[7] S. Sun, E.E. Fullerton, D. Weller, C.B. Murray, IEEE Trans. Magn. 37 (2001) 1239.
[8] H. Zeng, S. Sun, T.S. Vedantam, J.P. Liu, Z.-R. Dai, Z.-L. Wang, Appl. Phys. Lett. 80 (2002) 2583.
[9] S. Stappert, B. Rellinghaus, M. Acet, E.F. Wassermann, Mater. Res. Soc. Symp. Proc. 704 (2002) 73.
[10] H. Haberland, M. Karrais, M. Mall, Y. Thurner, J. Vac. Sci. Technol. A 10 (1992) 3266.
[11] S. Yamamuro, K. Sumiyama, K. Suzuki, J. Appl. Phys. 85 (1999) 483.
[12] C.-M. Kuo, P.C. Kuo, H.-C. Wu, J. Appl. Phys. 85 (2002) 2264.
[13] P.T.L. Minh, N.P. Thuy, N.D. Van, N.T.N. Chan, J. Magn. Magn. Mater. 239 (2002) 335.
[14] J. Urban, H. Sack-Kongehl, K. Weiss, Z. Phys. D 28 (1993) 247.
[15] S. Ino, J. Phys. Soc. Japan 21 (1966) 346;
S. Ino, S. Ogawa, J. Phys. Soc. Japan 22 (1967) 1365.
[16] H. Haberland, Clusters of Atoms and Molecules I and II, Springer, Berlin, 1995.
[17] T. Hihara, K. Sumiyama, J. Appl. Phys. 84 (1998) 5270.
[18] T. Hihara, K. Sumiyama, J. Vac. Sci. Technol. B 17 (1999) 1923.
[19] T. Sugimoto, Adv. Colloid Interface Sci. 28 (1987) 65.
[20] D.L. Peng, T. Hihara, K. Sumiyama, H. Morikawa, J. Appl. Phys. 92 (2002) 3075.